Sound speed and thermophysical properties of liquid iron and nickel

R. S. Hixson, M. A. Winkler, and M. L. Hodgdon
Los Alamos National Laboratory, Los Alamos, New Mexico 87545
(Received 27 April 1990)

An electrical-pulse-heating technique has been used to heat iron and nickel to high temperatures to measure thermophysical properties in the liquid state. A dynamic technique was used because static techniques, which are capable of greater precision, fail at a relatively low temperature. Measurements have been made, and results are shown for enthalpy, temperature, density, electrical resistivity, and sound speed up to 3950 K in iron and 4250 K in nickel.

I. INTRODUCTION

The use of pulse-heating techniques for the measurement of thermophysical data for several time regimes has been described previously.[1-3] These techniques are necessary in order to reach temperatures above about 2000 K where conventional static techniques become very difficult.

High-temperature data on the thermophysical properties of iron and nickel in the liquid phase are quite sparse. Since iron and nickel melt at temperatures (1810 K and 1728 K, respectively) that are relatively low, there are data close to the melting point because these temperatures are accessible by static techniques. Iron is an interesting metal to study because of its geological importance, and because it is ferromagnetic. The ferromagnetic properties of iron and nickel make them relatively difficult to study using our dynamic-pulse-heating technique. In particular, the ferromagnetism of iron and nickel causes the current diffusion times for uniform heating to be longer than for nonferromagnetic metals. In this paper we will show that there is still sufficient time for uniform heating of our iron and nickel samples. Our experimental apparatus has previously been described,[4] and results for several thermophysical properties have been reported for many nonferromagnetic materials.[5-7] In this paper we report our measurements of sound velocity, enthalpy, density, temperature, and electrical resistivity up to 3950 K for iron and 4250 K for nickel. These temperatures represent the stability limits for pulse heating these two metals.

II. EXPERIMENTAL DETAILS

Specimens were cut from 0.75-mm-diameter wire, and were of 99.99% purity. Samples were highly polished and approximately 25-mm long. Our experimental apparatus consists of a gas high-pressure vessel, associated pumping equipment, and a high-energy capacitor bank (50 kJ at 20 kV) to provide heating current. Electrical diagnostics measure current through the sample and voltage along a sample length defined by two probes. Several optical diagnostics are used to measure other properties. An argon-ion laser backlights the sample, creating a shadow of the sample diameter, which is imaged onto a slit. An image converter streaking camera is focussed onto the slit plane, and a time-resolved record of the sample diameter is obtained. From this streak the sample density can be calculated during an experiment. By combining the measured current, voltage, and density, we can calculate enthalpy and electrical resistivity:

$$H(t)=\int_{t_0}^{t} I(t)V(t)dt \ ,$$

$$\rho_{\rm el}(t)=A(t)R(t)/l \ .$$

Here H is enthalpy, I is current, V is voltage, $\rho_{\rm el}$ is electrical resistivity, A is the cross-sectional area of the sample, $R=V/I$ is the sample resistance, and l is the voltage probe spacing.

Sound speeds are measured as described previously[8] using a noncontacting technique. A pulsed ruby laser ($\sim$0.1 J with 30-ns pulse length) is focused into a small spot ($\sim$0.1-mm diameter), driving a low-amplitude, spherically diverging stress wave into the sample. This disturbance quickly attenuates into a sound wave and propagates across the sample diameter, allowing the transit time to be measured. The sound speed is measured using the same line of sight as for the volume measurement, with data recorded using the image converter streaking camera. Our method for measuring sound velocities is limited in accuracy to an estimated $\pm 5\%$. On a given experiment the diameter of the sample is measured from the streak image, and the transit time is measured as described above, yielding an average sound speed. It is essential that sample motion be kept to a minimum during the heating phase of an experiment in order to maintain the ruby laser alignment, and so great care is taken in the sample preparation.

Temperatures are measured using an optical pyrometer of a design previously discussed.[6] For this work a single channel has been used at $\lambda=700$ nm. Since the melting points of both iron and nickel are below our pyrometer response, we have used a temperature-enthalpy tie point to calculate temperatures. This tie point was found by extrapolating the work of Vollmer *et al.*[9] to a temperature of 2300 K. Temperature uncertainties were estimated to be $\pm 5\%$.

III. EXPERIMENTAL RESULTS

A. Iron results

Two kinds of experiments were performed on iron specimens. In the first series of experiments samples were pulse heated in an argon gas atmosphere at a pressure of 2 kbar and volume, current, voltage, and temperature were measured. From these quantities enthalpy, density, electrical resistivity, and specific heat, C_p, were calculated. In the second kind of experiment sound speed was measured. Our results for iron are summarized in Table I.

Shown in Fig. 1 is plot of enthalpy against temperature. The least-squares fit to these data is given by

$$H = 8.1537 \times 10^{-4} T - 0.22846 \quad (1)$$

for $2125 \leq T \leq 3950$ K, where H is in MJ/kg. From this fit a value of 815.4 J/kg K is found for C_p, the specific heat at constant pressure. This is in reasonable agreement with the value of Pottlacher *et al.*[10] of 929.3 J/kg K, that of Trevorton and Margrave[11] of 763.0 J/kg K, and that of Vollmer *et al.*[9] of 824.1 J/kg K. Enthalpy is the most accurate of all properties measured with estimated uncertainties of ±2%.

Our values for volume, converted to density and plotted against temperature are shown in Fig. 2. Also shown are the static measurements of Drotning *et al.*[12] The agreement is quite good. The best fit to our data is given by

$$\rho = -0.64985T + 8.171 \times 10^3 \quad (2)$$

for $2125 < +T \leq 3950$ K. Densities may also be fit against enthalpy, and the result is

$$\rho = -797.353H + 7.9903 \times 10^3 \quad (3)$$

for $1.5 \leq H \leq 3.0$ MJ/kg. Using the fits above it is possible to calculate

$$\alpha = -\frac{1}{\rho}\left[\frac{\partial \rho}{\partial T}\right]_p ,$$

the thermal expansion coefficient, and this is shown for our data in Fig. 3. Also shown are values of α calculated from the data of Drotning *et al.*, which are in good agreement with our data. The error bars on the calculated values of α are estimated to be ±10% or more.

Electrical resistivities may be calculated from our data, with the results shown in Fig. 4, plotted against enthalpy. The least-squares fit to this data is

$$\rho_{el} = 22.87941H - 117.0463 , \quad (4)$$

where $1.5 \leq H \leq 3.0$ MJ/kg K, and ρ_{el} is in $\mu\Omega$ cm. The agreement with the data of Pottlacher *et al.*[10] is not

TABLE I. Thermophysical properties of liquid iron.

H (MJ/kg)	T(K)	ρ (10^3 kg/m^3)	V/V_0	ρ_{el} ($\mu\Omega$ cm)
1.5	2125	6.85	1.148	150.5
1.6	2250	6.75	1.164	153.3
1.7	2340	6.64	1.184	156.0
1.8	2490	6.54	1.202	158.0
1.9	2600	6.40	1.229	161.3
2.0	2735	6.34	1.240	163.7
2.1	2860	6.29	1.250	165.1
2.2	2990	6.22	1.263	167.2
2.3	3100	6.15	1.278	170.3
2.4	3230	6.07	1.295	172.4
2.5	3360	6.02	1.305	174.1
2.6	3475	5.98	1.315	175.1
2.7	3585	5.90	1.333	178.2
2.8	3710	5.80	1.355	181.0
2.9	3835	5.65	1.393	183.4
3.0	3950	5.54	1.420	186.0

$\rho_0 = 7.86 \times 10^3$ kg/m^3.
$P_c = 2$ kbar.

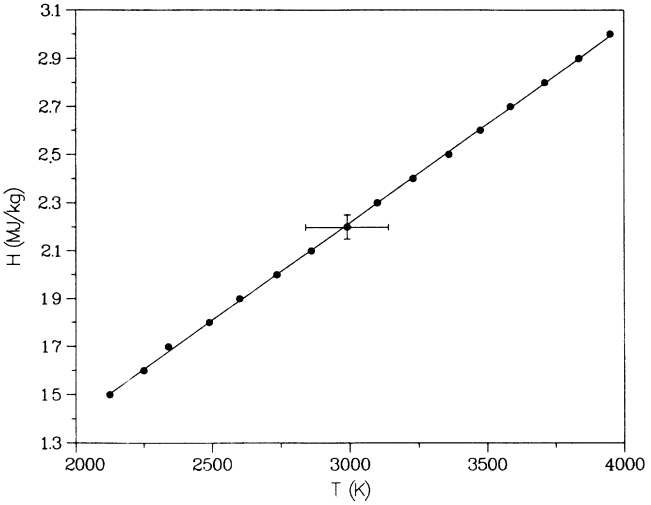

FIG. 1. Measured enthalpies for liquid iron plotted against temperature.

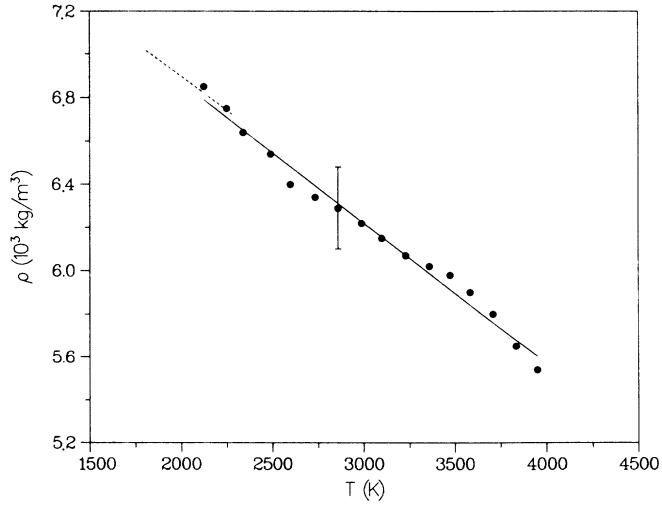

FIG. 2. Densities for liquid iron plotted against temperature (●) shown with the best fit (——). Also shown is the fit given by Drotning (Ref. 12) for his data (— — —).

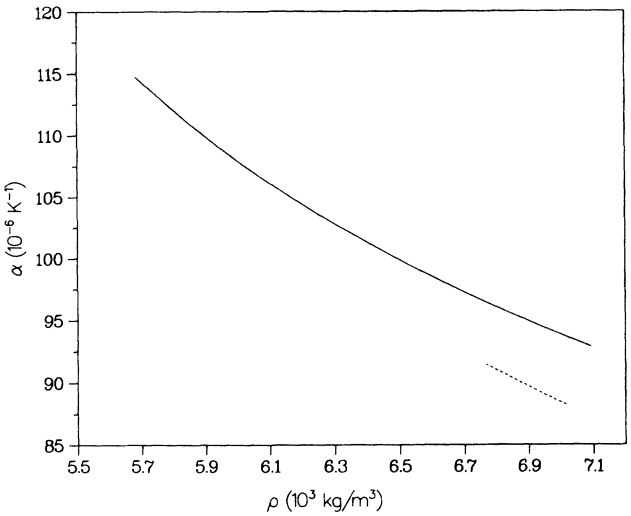

FIG. 3. Calculated values for thermal expansion coefficient α for iron (——) shown with values calculated from the data of Drotning (Ref. 12) (— — —).

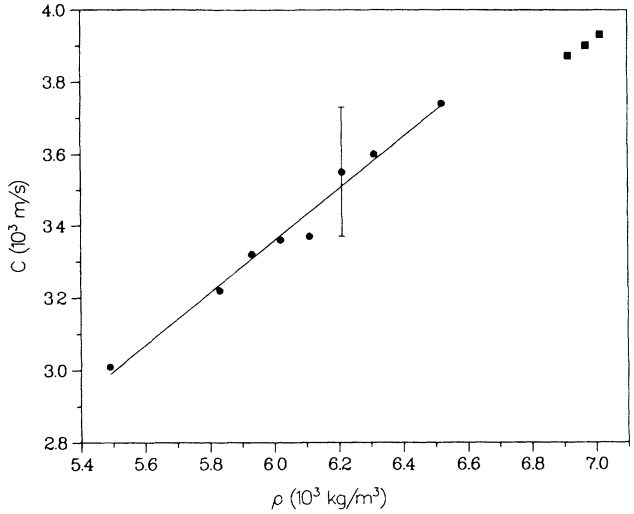

FIG. 5. Our measured values of sound speed for liquid iron (●) shown with the best fit. Also shown are values measured by Kurtz and Lux (Ref. 14) (■).

good, and part of this may be due to the volume corrections used by Pottlacher.[13] The estimated accuracy of ρ_{el} is ±4%.

Our measured values for sound speed in liquid iron are shown in Fig. 5, plotted against density. It can be seen that sound speed is linear with density, and the least-squares fit is

$$c = 0.7326\rho - 983.4 \ , \tag{5}$$

where c is in m/s.

Also shown in Fig. 5 is the static data of Kurtz and Lux,[14] which is in close agreement with our data. Sound speeds that are linear with density have been found for many other metals, and this behavior has been discussed previously by Birch.[15]

By combining the above results we may now calculate the thermodynamic properties of molten iron. We define

$$B_s = \rho c^2 \ ,$$

the adiabatic bulk modulus, and then calculate $K_s = 1/B_s$ the adiabatic compressibility.

The value of Grüneisen gamma may be found from

$$\gamma_G = \frac{\alpha C^2}{C_p} \ ,$$

and the results are plotted in Fig. 6. The error bars on γ_G are ±20% or more.

The specific heat at constant volume $C_v = (\partial E/\partial T)_v$ may be found, with relatively large error bars (~±20%),

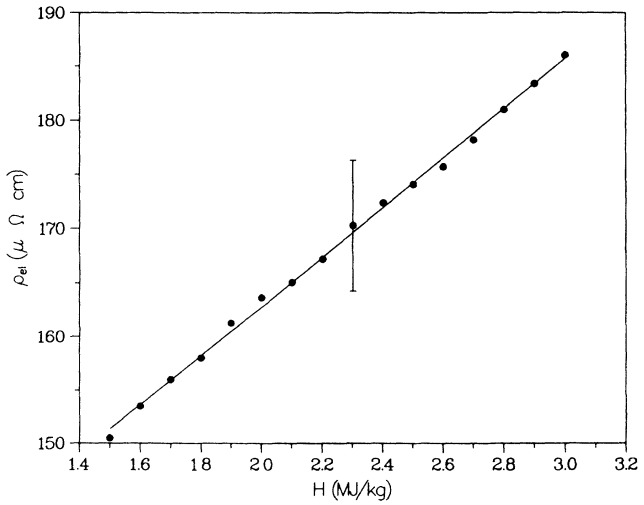

FIG. 4. Measured values of electrical resistivity for liquid iron.

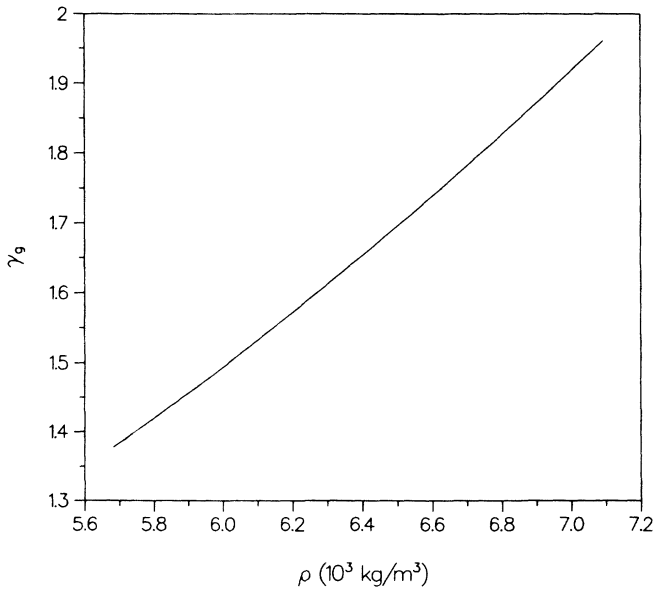

FIG. 6. Values of Grüneisen parameter, γ_G, calculated from our data for liquid iron.

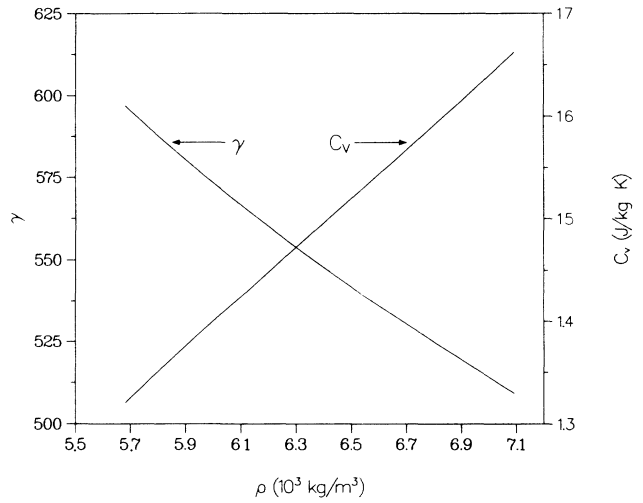

FIG. 7. Calculated values for specific heat at constant volume C_V and $\gamma = C_p/C_V$ for liquid iron.

in terms of other measured and calculated properties from

$$C_v = \frac{C_p^2}{C_p + \alpha^2 T_c} .$$

The results of this calculation and the values for the thermodynamic $\gamma = C_p/C_v$ are shown in Fig. 7. Now that we have γ we can calculate

$$B_T = B_s/\gamma ,$$

the isothermal bulk modulus. The calculated values for B_T and $K_T = 1/B_T$, the isothermal compressibility are shown in Fig. 8.

B. Nickel results

The measurements for nickel were done the same way as those for iron, and the results are summarized in Table II for the 2-kbar isobar.

TABLE II. Thermophysical properties of liquid nickel.

H (MJ/kg)	T(K)	ρ (10^3 kg/m^3)	V/V_0	ρ_{el} ($\mu\Omega$ cm)
1.2	1906	7.71	1.154	97.31
1.3	2045	7.57	1.176	97.29
1.4	2183	7.48	1.190	98.17
1.5	2321	7.48	1.190	99.96
1.6	2460	7.45	1.195	101.70
1.7	2598	7.38	1.206	102.50
1.8	2736	7.30	1.220	105.99
1.9	2875	7.24	1.230	106.52
2.0	3013	7.12	1.250	109.11
2.1	3151	7.00	1.270	111.41
2.2	3290	6.87	1.295	113.40
2.3	3428	6.73	1.323	114.00
2.4	3566	6.64	1.340	115.52
2.5	3704	6.57	1.354	116.71
2.6	3843	6.44	1.382	
2.7	3981	6.36	1.400	
2.8	4119	6.36	1.400	
2.9	4258	6.24	1.427	

$\rho_0 = 8.9 \times 10^3$ kg/m^3.
$P_0 = 2$ kbar.

Our results for enthalpy and temperature are plotted in Fig. 9, with the least-square fit

$$H = 7.2299 \times 10^{-4} T - 0.178\,324 \qquad (6)$$

for $1.2 \le H \le 2.9$ MJ/kg. This leads to a specific-heat value $C_p = 723$ J/kg K. Other measured values of C_p for liquid nickel are those of 761 J/kg K by Pottlacher *et al.*[10] of 741 J/kg K by Margrave,[16] and of 743 J/kg K by Vollmer *et al.*[9]

Our measured values for density are shown in Fig. 10 plotted against temperature, with the results of Drotning *et al.*[12] shown for comparison. The best fit to this data is

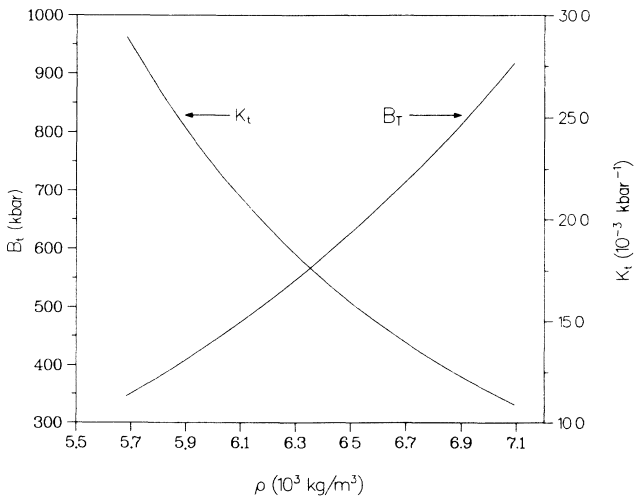

FIG. 8. Calculated values of isothermal bulk modulus B_t and compressibility K_t for liquid iron.

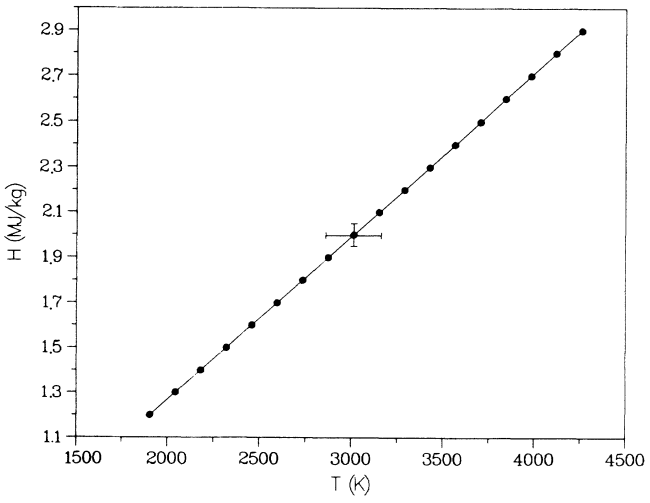

FIG. 9. Measured values of enthalpy for liquid nickel shown plotted against temperature.

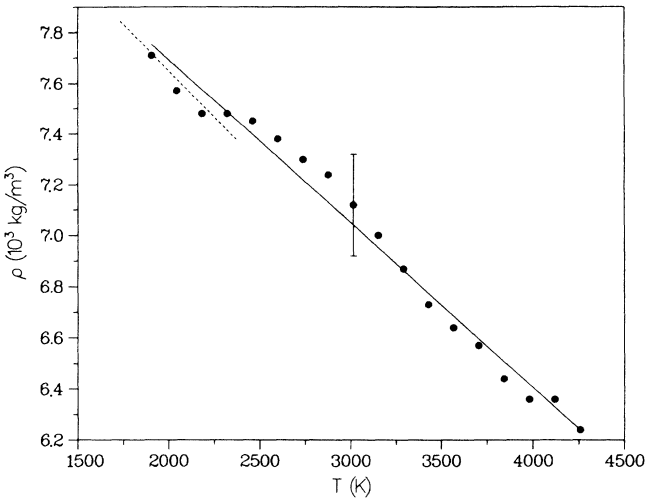

FIG. 10. Measured densities for liquid nickel (●) shown with the best fit (——). Also shown is the fit given by Drotning (Ref. 12) for their data (— — —).

given by

$$\rho = -0.644\,06T + 8.9817\times 10^3 \tag{7}$$

for $1906 \le T \le 4258$ K. The best fit to densities in terms of enthalpy are given by

$$\rho = -890.8151H + 8.8228\times 10^3 \tag{8}$$

for $1.2 \le H \le 2.9$. For both of these fits ρ is in kg/m^3 and H is in MJ/kg.

Electrical resistivities have been calculated as described above for iron, and the best fit to this data is given by

$$\rho_{\rm el} = 16.4251H + 76.0652 \ , \tag{9}$$

where $\rho_{\rm el}$ is in $\mu\Omega$ cm and $1.2 \le H \le 2.5$ MJ/kg. Data for liquid nickel have also been measured by Pottlacher *et al.*,[10] and their measured values are in poor agreement with our results.

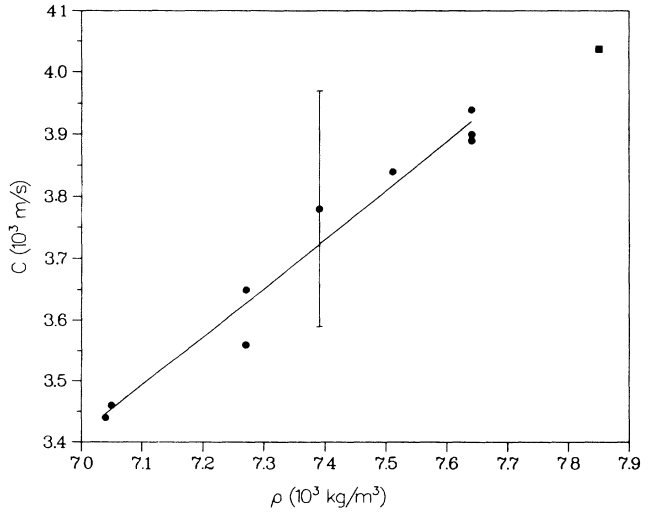

FIG. 11. Measured values of sound speed in liquid nickel (●) shown with the best fit (——). Also shown (■) is a data point at melt taken from Keita *et al.* (Ref. 17).

Sound velocity measurements have been made in liquid nickel, and our results are shown in Fig. 11 compared with a point at the melting temperature measured by Kieta *et al.*[17] The least-squares fit to our data is given by

$$c = 0.7915\rho - 2.1265 \tag{10}$$

for $7.0\times 10^3 \le \rho \le 7.6\times 10^3$ kg/m^3.

IV. DISCUSSION

The pulse-heating technique that we use to measure thermophysical properties of metals has been used on many nonferromagnetic metals, and is proven to be able to heat a wire-shaped sample very uniformly. Hodgson[18] has shown for a lead sample the skin depth is roughly 0.5 mm, so a sample diameter of 1 mm is ideal. We need to address the problem of applying the pulse-heating method to a strongly ferromagnetic material such as iron, and see how a uniform heating can take place.

From the diffusion equation governing the current density in a homogeneous, isotropic slab of material of constant permeability μ and constant resistivity $\rho_{\rm el}$,

$$\nabla^2 j - \frac{\rho_{\rm el}}{\mu}\frac{\partial j}{\partial t} = 0 \ ,$$

we note that the diffusivity, $\rho_{\rm el}/\mu$, varies inversely with permeability. Although in ferromagnetic materials μ is not constant, the values of μ in nonsaturated ferromagnetic materials usually exceed that of the free space permeability μ_0. This suggests that the current will take longer to reach the center of a wire of iron or nickel than a wire of a nonmagnetic material.

In order to determine the diffusion times in our experiments, we computed the time history of the current density in a 0.75-mm wire of iron using the finite-element code FLUX2D.[19] With FLUX2D we are able to take into account the cylindrical geometry, the temperature dependence of the resistivity, the magnetic hysteresis, and the transient local heating.

In FLUX2D, the current density is calculated from the magnetic vector potential A as

$$j(x,t) = \nabla\times\nabla\times \mathbf{A}(x,t) \ , \tag{11}$$

where $\mathbf{A}$ satisfies the equation

$$\nabla\times\left[\frac{1}{\mu}\nabla\times\mathbf{A}\right] + \frac{1}{\rho_{\rm el}}\frac{\partial \mathbf{A}}{\partial t} = \frac{\mu_0 I(t)}{2\pi r^2} \ . \tag{12}$$

Here, $I(t)$ is the input current at time t, r is the radius of the wire, μ is the local permeability, and $\rho_{\rm el}$ is the resistivity which varies with temperature as

$$\rho_{\rm el} = 8.57 + 9.136\times 10^{-2} T \tag{13}$$

for $T < 1200$ K,[20] and ρ_e is in $\mu\Omega$ cm.

The temperature T is computed from the thermal diffusion equation,

$$-\nabla(k\nabla T) + c_p\frac{\partial T}{\partial t} = j^2\rho \ , \tag{14}$$

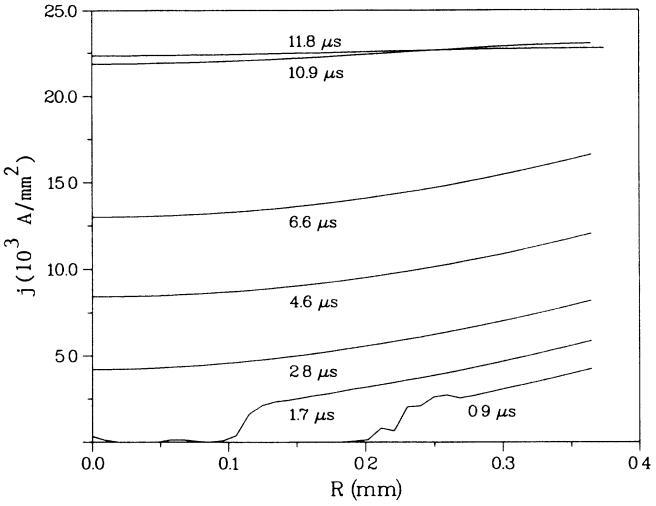

FIG. 12. Calculated current densities as a function of sample radius for a ferromagnetic conductor at several times during the heating cycle. It can be seen that a uniform current distribution takes longer in the ferromagnetic case than in the nonferromagnetic case, shown in Fig. 13.

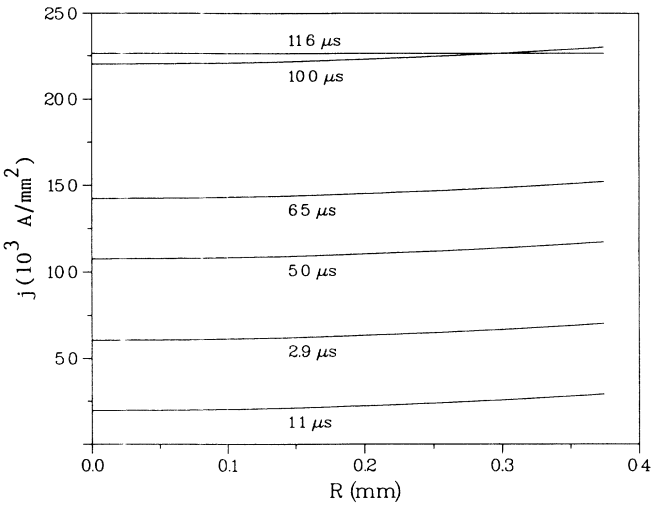

FIG. 13. Calculated current densities as a function of sample radius within a nonferromagnetic conductor under the same conditions as the calculation of Fig. 13.

where the heat source $j^2\rho$ is given in Eqs. (11)–(13), the thermal conductivity k in W/m K is given by[20]

$$k = 98.99 - 8.72\times10^{-2}\,T + 2.18 + 10^{-5}\,T^2\,, \qquad (15)$$

and the specific heat in J/cm^3 K is[21]

$$c_p = 2929 + 0.495T - 8.975\times10^{-4}\,T^2 + 5.62\times10^{-7}\,T^3 - 3.23\times10^{-1}\,T^4\,. \qquad (16)$$

We considered two forms for μ. In the first, the value of μ is set to that of the free space permeability. In the second, μ is the derivative of the dc initial magnetization curve. Since hysteresis is rate dependent, it would be appropriate to use a magnetization curve measured under the time conditions of the experiment. In general, such high-rate hysteresis curves show similar saturation behavior but a much more gradual approach to saturation and, hence, a much lower peak permeability than the dc curve. Thus, the use of the dc permeabilities provides a worst case calculation.

The set of Eqs. (11)–(16) were solved in FLUX2D at time intervals of about 0.2 μs from the time $t = 0$ to $t = 10$ μs during which the current increases linearly from 0 to 10^4 amps. From $t = 10$ μs until $t = 15$ μs, the current was held at this maximum value and the calculations were made at intervals of approximately 0.5 μs. From the results shown in Fig. 12, we find that the current density is fairly uniform over the ferromagnetic wire by about 11 μs. This is a considerably longer diffusion time than for the case in Fig. 13 of the nonmagnetic wire, but it is still within the time interval of interest for the experiment. These results are highly dependent on the sample size, and on the magnitude of the current, which here is sufficient to saturate the material and cause the permeability to decrease eventually to μ_0.

ACKNOWLEDGMENTS

We wish to thank Professor M. Manghani for suggesting this work, and we wish to thank G. C. Powley for his assistance in the experiments and data analysis. This work was supported by the U.S. Department of Energy.

[1]G. R. Gathers, J. W. Shaner, and R. K. Brier, Rev. Sci. Instrum. **47**, 471 (1976).
[2]A. Cezairiyan, J. Res. N.B.S. **75C**, 7 (1971).
[3]U. Seydel and W. Fucke, Naturforsch. Teil A **32**, 994 (1977).
[4]R. S. Hixson, M. A. Winkler, and J. W. Shaner, Physica **139**, 893 (1986); **140B**, 893 (1986).
[5]R. S. Hixson, M. A. Winkler, and J. W. Shaner, High Temperature/High Pressure **18**, 635 (1986).
[6]R. S. Hixson and M. A. Winkler, Int. J. Thermophys. **11**, 709 (1990).
[7]R. S. Hixson and M. A. Winkler, High Press. Res. **4**, 555 (1990).
[8]R. S. Hixson, M. A. Winkler, and J. W. Shaner, High Temp. High Pressures **17**, 267 (1985).
[9]O. Vollmer, R. Kohlhaas, and M. Braun, Z. Naturforsch. **21**, 181 (1966).
[10]G. Pottlacher, H. Jäger, and T. Neger, High Temp. High Pressures **19**, 19 (1987).
[11]J. A. Treverton and J. L. Margrave, J. Chem. Thermodyn. **3**, 473 (1971).
[12]W. D. Drotning, High Temp. High Pressures **13**, 441 (1981).
[13]G. Pottlacher (private communication).
[14]W. Kurz and B. Lux, High Temp. High Pressures **1**, 387 (1969).

[15]F. Birch, Phys. Earth Planet. Inter. **1**, 141 (1968).
[16]J. L. Margrave, High Temp. High Pressures **2**, 583 (1970).
[17]N. M. Keita, H. Morita, and S. G. Steinemann, *Proceedings of the 4th International Conference on Rapidly Quenched Metals, Sendai, 1981* (The Japan Institute of Metals, Sendai, 1982) Vol. 119.
[18]W. M. Hodgson, Ph.D. thesis, UCRL-52493, University of California, 1978.
[19]J. C. Sabonnadiére and J. L. Coulomb, *Finite Element Methods in CAD: Electrical and Magnetic Fields* (Springer, Berlin, 1987).
[20]Y. S. Touloukian and E. H. Buyco, *Thermophysical Properties of Matter* (Plenum, New York, 1970), Vol. 1.
[21]Y. S. Touloukian and E. H. Buyco, *Thermophysical Properties of Matter* (Plenum, New York, 1970), Vol. 4.